Neural Computing and Applications (2023) 35:23329–23341
https://doi.org/10.1007/s00521-021-06037-z

SPECIAL ISSUE ON HUMAN-IN-THE-LOOP MACHINE LEARNING AND ITS APPLICATIONS

Iterative learning-based path control for robot-assisted upper-limb rehabilitation

Kamran Maqsood[1] · Jing Luo[2] · Chenguang Yang[3] · Qingyuan Ren[4] · Yanan Li[1]

Received: 5 October 2020 / Accepted: 13 April 2021 / Published online: 2 May 2021
© The Author(s) 2021

Abstract
In robot-assisted rehabilitation, the performance of robotic assistance is dependent on the human user's dynamics, which are subject to uncertainties. In order to enhance the rehabilitation performance and in particular to provide a constant level of assistance, we separate the task space into two subspaces where a combined scheme of adaptive impedance control and trajectory learning is developed. Human movement speed can vary from person to person and it cannot be predefined for the robot. Therefore, in the direction of human movement, an iterative trajectory learning approach is developed to update the robot reference according to human movement and to achieve the desired interaction force between the robot and the human user. In the direction normal to the task trajectory, human's unintentional force may deteriorate the trajectory tracking performance. Therefore, an impedance adaptation method is utilized to compensate for unknown human force and prevent the human user drifting away from the updated robot reference trajectory. The proposed scheme was tested in experiments that emulated three upper-limb rehabilitation modes: zero interaction force, assistive and resistive. Experimental results showed that the desired assistance level could be achieved, despite uncertain human dynamics.

Keywords Adaptive impedance control · Trajectory learning · Path control · Human–robot interaction · Robot-assisted rehabilitation

1 Introduction

According to the World Health Organization (WHO), each year around eight million people suffer from upper-limb motor dysfunctions [1]. One of major means of recovery is after-stroke rehabilitation [2], which uses various training modes according to human patients' recovery stages [3, 4]. Over the last few decades, robot-assisted rehabilitation (RAR) has gained considerable interest and proved its effectiveness to address motor dysfunction [5].

In RAR, regulation of physical human–robot interaction (pHRI) plays a key role in improving human patients' recovery [6] and more technically, it affects the stability and performance of HRI systems [7–9]. Therefore, various control techniques have been introduced for RAR, including impedance control, position control and force control [10–13]. Due to its inherent robustness, impedance control has been explored extensively in the literature for pHRI and particularly RAR [6, 14–16]. One challenge of using impedance control-related approaches is how to obtain optimal impedance parameters that determine the relationship between the interaction force and position [17, 18]. By choosing the robot's impedance parameters, it can provide corresponding assistance to the human users. For example, stiff interaction with high impedance is

K. Maqsood and J. Luo: The first two authors contributed equally to the work.

✉ Yanan Li
yl557@sussex.ac.uk

[1] Department of Engineering and Design, University of Sussex, Brighton BN1 9RH, UK

[2] The School of Electrical and Information Engineering, Changsha University of Science and Technology, Changsha 410114, China

[3] The Bristol Robotics Laboratory, University of the West of England, Bristol BS16 1QY, UK

[4] The State Key Laboratory of Industrial Control Technology, Zhejiang University, Hangzhou 310058, China

desirable to assist human users with little arm function. Conversely, excessive assistance from the robot is not beneficial to promote human users' recovery. These problems motivate researchers towards variable impedance control, aiming to design adaptive impedance approaches to maintain a desired level of pHRI [19, 20]. An adaptive impedance controller was developed in [21], where surface electromyography (sEMG) signals were used to obtain the optimal reference impedance parameters for an upper-limb robotic exoskeleton. In [22], minimal-intervention-based admittance control was developed to improve the degree of participation and maximize the effects of motor function training for patients. In the context of RAR, in this paper we will develop an adaptive impedance method to guarantee the robot's tracking capability in the presence of external disturbance, including the interaction forces generated by unintentional human movements.

Besides impedance parameters, the robot's reference trajectory is another open factor that can be designed to regulate the pHRI. In early research works, predefined reference trajectories were usually used [23]. Recent researches have looked into the update of robot's reference trajectory in order to improve pHRI [24, 25]. In [26, 27], the rehabilitation robot updated its trajectory or followed the target trajectory in response to the change of human partner's interaction profiles, such as force and torque. In [28], a therapist-in-the-loop framework was introduced to adjust the desired trajectory for the patients when it is unsuitable. Despite these works, a systematic framework to automatically update the robot's reference trajectory in the presence of uncertain human dynamics is still missing [29]. In this paper, we explore iterative learning control (ILC) given the repetition nature of rehabilitation tasks.

ILC is a well-established control approach suitable for repetitive tasks and it has been used to cope with the uncertainties and unknown dynamics in various motion control systems. In [30], ILC was used to model human learning in repetitive tasks. In [31], online linear quadratic regulator based on ILC was proposed to determine the optimal weight matrix for trajectory tracking. In [32], a passivity-based ILC approach was developed to guarantee the convergence of the tracking error. In this paper, we propose a novel approach to use ILC for the rehabilitation robot's controller design, by updating the robot's reference trajectory for the next cycle according to the interaction force in the current one. In the presence of uncertainty and without requirement of knowledge of human dynamics, the proposed method is able to achieve a constant level of assistance to the human by repeating the rehabilitation exercise, represented by a predefined desired interaction force. As the proposed approach is based on ILC, its learning convergence can be explicitly proved, which is essential to ensure the desired level of interaction.

Noticing the fact that a human user needs assistance in their movement direction but constraint in other directions in order to achieve accurate task path tracking, we divide the task space into two subspaces with different control strategies. In a 2-dimensional case, the aforementioned adaptive impedance control is implemented to constrain the human user onto a predefined task path, while trajectory learning is implemented in the direction along the task path to provide a desired level of assistance to the human user. For this purpose, we adopt the coordinate transformation method in contouring control [33–35], where the robot's reference frame is attached to its own reference trajectory with an axis along the trajectory and the other normal to it. Therefore, the proposed approach achieves both assistance and constraints to the human movement, in the context of RAR.

The main context of the proposed approach in this paper is summarized as below.

- Adaptive impedance control is introduced to ensure the tracking performance of the rehabilitation robot. An update law is developed to regulate the robot's impedance parameters to cope with the unknown disturbance from the external environment and human user's unintentional movement.
- Trajectory learning is proposed to provide a constant level of assistance with a desired force to the human user, in the presence of uncertain and unknown human dynamics. A learning law is developed by using the interaction force to update the robot's reference trajectory. Due to the nature of rehabilitation exercise and ILC, the learning convergence can be achieved without the knowledge of human dynamics that are typically different from one human user to the other.
- A task frame with reference to the robot's reference trajectory is defined, so that the above two control strategies can be implemented in two separate subspaces to provide both assistance and constraints to the human movement. It merges the idea of contouring control in motion control systems and provides a new direction of controller design for pHRI applications.

Compared to related works in the literature, the novelties of the proposed approach are threefold: an impedance adaptation method is proposed to compensate for unknown human force and assist the human user to follow the task trajectory; a new trajectory learning method is developed to achieve a desired assistance force, which addresses the problem of unknown human movement speed; and an online motion planning framework is proposed to allow the robot to achieve two independent control objectives in two subspaces.

Section 2 presents the problem formulation and preliminaries about coordinate transformation. Section 3

describes the proposed controller with adaptive impedance control and trajectory learning in two subspaces. The experimental results are presented in Sect. 4. Finally, the conclusion and future work are summarized in Sect. 5. For the convenience of the readers, related notations are summarized in Table 1.

2 Problem formulation and preliminaries

2.1 Problem formulation

An upper-limb rehabilitation scenario is illustrated in Fig. 1, where a human hand holds a handle (the robot's end-point) to carry out a predefined exercise, e.g. following a circular path. The robot is able to provide assistance forces to the human hand, whose levels can be predefined according to the human user's recovery stages, e.g. a large assistance force for a user who can barely move their arm and a small one for a user who can complete the task partially. While the robot has prior knowledge of the task path, it does not know the human user's movement pattern, e.g. human speed.

Table 1 Nomenclature

X_o	Robot's actual position in the world frame
X_{od}	Robot's predefined desired position in the world frame
X	Robot position
X_t	Robot position in the tangential direction
X_{hd}	Desired human trajectory
X_d	Desired robot trajectory in the tangential direction
X_{vt}	Virtual trajectory in the tangential direction
X_{hdt}	Desired human trajectory in the tangential direction
m	Unit tangent vector
n	Unit normal vector
p	Unit binormal vector
e_o	Tracking error in the world frame
e_{oc}	Contouring error
e	Tracking error in the task frame
e_n	Tracking error in the tangential direction
e_c	Contouring error in the task frame
e_t	Tracking error in the normal direction
R	Transformation matrix
u	Robot's control input
u_1	Feed-forward term
u_2	Feedback term
u_3	Adaptive impedance term
f_h	Human force applied to the robot
f_d	Disturbance force
f_{ht}	Human force in the tangential direction
f_{hdt}	Desired human force in the tangential direction
K_h	Human arm stiffness
K_{d1}, K_{d2}	Unknown disturbance parameters
K_p, K_d	Robot's feedback gains
K, D	Robot's adaptive impedance matrices
θ_k, θ_d	Positive parameters
ϕ	Positive learning rate

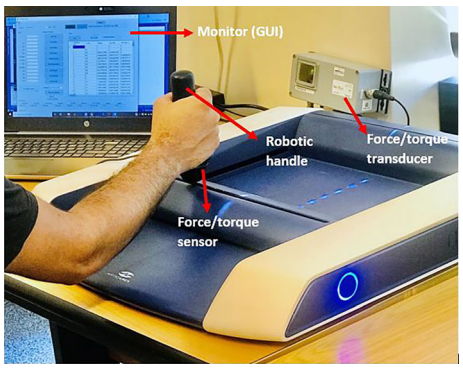

Fig. 1 A scenario of robot-assisted upper-limb rehabilitation

In this scenario, we mainly consider two objectives that a typical rehabilitation robot should achieve. First, the robot should provide a desired level of assistance to the human user in the direction along the predefined path, which is quantified by the interaction force between the robot and the human hand. Second, the robot should assist the human user to stay onto the path when their hand drifts away, e.g. due to hand trembling. These two control objectives can be achieved in two separate subspaces divided with reference to the predefined path. As shown in a 2-dimensional case in Fig. 2, the robot's task space can be defined by a coordinate frame attached to the predefined path, with one axis normal to the path and the other tangential.

With the robot's task frame defined, two controllers will be, respectively, designed in two directions: a position controller in the direction normal to the path and a force

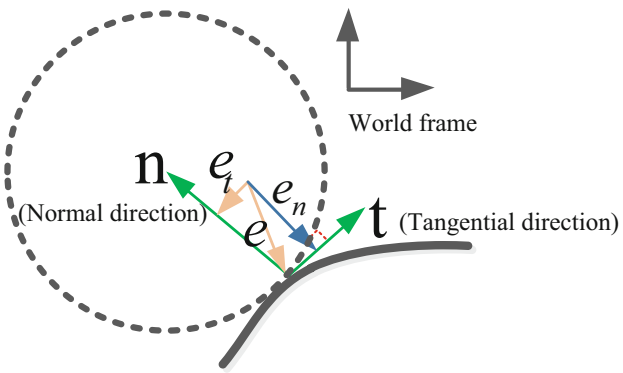

Fig. 2 A coordinate frame attached to the predefined task path, whose one axis is along the path and the other normal to the path

controller along the path. However, the design of these two controllers is nontrivial. For the position controller, the robot is subject to external disturbance and unintentional human movement, so we will develop an adaptive impedance controller to address these issues. For the force controller, as human movement and dynamics are different in each individual, we propose an ILC-based learning method to update the robot's reference trajectory according to the interaction force, without requirement of human model and relying on the repetition nature of the rehabilitation exercise.

2.2 Preliminaries

This section introduces the preliminaries about the coordinate transformation from a world frame to the frame attached to the task path, which will facilitate the controller design in the following section.

2.2.1 Contouring error

We start with introducing contouring error, which has been mainly studied in the literature of motion control [36]. Without considering the orientation of the robot's endpoint, its actual position in the original world frame is defined as

$$X_o = [x, y, z]^T. \tag{1}$$

The robot's predefined desired position in the world frame is

$$X_{od} = [x_d, y_d, z_d]^T. \tag{2}$$

Thus, the tracking error in the world frame is

$$e_o = [x - x_d, y - y_d, z - z_d]^T. \tag{3}$$

The contouring error e_{oc} is the minimal distance between the actual position and the desired path, defined as

$$e_{oc}(x) = \min |[x - x_d, y - y_d, z - z_d]|. \tag{4}$$

From the above definition, we find that it is nontrivial to compute the contouring error, which in many cases does not have an analytic solution. In this paper, we adopt a first-order method to approximate the contouring error [36], which will be detailed in the following subsection.

2.2.2 Coordinate frame transformation

Given the desired trajectory X_{od}, the following unit vectors can be computed:

$$m = \frac{\dot{X}_{od}}{|\dot{X}_{od}|}, \; n = \frac{\dot{m}}{|\dot{m}|}, \; p = m \times n \tag{5}$$

where m is a unit tangent vector, n is a unit normal vector and p is a unit binormal vector. Then, a transformation matrix is obtained as

$$R = [m, n, p] \tag{6}$$

which can be used to transform e_o from the world frame to the task frame, defined as

$$e = Re_o \tag{7}$$

where e is the tracking error in the task frame corresponding to e_o. When the desired position X_{od} is close to the actual position X_o, the contouring error e_{oc} can be approximated by the normal and binormal components of e_o. In a 2-dimensional case, the contouring error can be approximated by the projection of the tracking error to the normal direction, i.e.

$$e_c \approx e_n \tag{8}$$

where e_n is the tracking error in the normal direction, as a component of

$$e = \begin{bmatrix} e_t \\ e_n \end{bmatrix} \tag{9}$$

with e_t as the tracking error in the tangential direction.

As the contouring error is approximated by the tracking error in the normal direction, we can design a position controller to reduce this error so that the human movement will be constrained to the desired path. In the tangential direction, a force controller can be designed to achieve a desired level of assistance to the human user. In this way, the robot's task space is divided into two subspaces, with two controllers to be developed independently.

3 Controller design

3.1 System dynamics

The dynamics model of a planar rehabilitation robot is given as

$$M_d\ddot{X} + B_d\dot{X} = u + f_h + f_d \tag{10}$$

where M_d and B_d are positive definite inertia matrix and damping matrix, respectively, u is the robot's control input, f_h and f_d are the human force applied to the robot and the disturbance force, respectively.

For analysis purpose, the human force can be modelled as

$$f_h = K_h(X - X_{hd}) \tag{11}$$

where K_h is the human arm stiffness and X_{hd} is the desired position of the human arm's endpoint. Since the human user performs repetitive rehabilitation exercises, X_{hd}

corresponds to the predefined task path so it is assumed to be periodic with a task duration T. Note that these parameters will not be used in the robot's controller.

We also consider a disturbance force due to external environment or human's unintentional movement, modelled as

$$f_d = K_{d1}(X - X_d) + K_{d2}(\dot{X} - \dot{X}_d) \tag{12}$$

where K_{d1}, K_{d2} are unknown constant matrices, X_d is the desired trajectory of the robot's end-effector. This model shows that the disturbance force makes the robot diverge from its reference trajectory.

3.2 Robot controller

The robot's controller is designed as

$$u = u_1 + u_2 + u_3 \tag{13}$$

where u_1 is the feed-forward term to compensate for the robot's dynamics, u_2 is the feedback term to guarantee the stability when there is no disturbance and u_3 is the adaptive impedance term to deal with the unknown disturbance f_d. They are, respectively, designed as

$$u_1 = M_d\ddot{X}_d + B_d\dot{X}_d - f_h \tag{14}$$

$$u_2 = -K_p e - K_d\dot{e} \tag{15}$$

where K_p and K_d are the robot's feedback gains, and

$$u_3 = -Ke - D\dot{e} \tag{16}$$

where K and D are the robot's adaptive impedance matrices. Combining Eqs. (10)–(16), the dynamics of the closed-loop system can be written as

$$M_d\ddot{e} + B_d\dot{e} = -K_p e - K_d\dot{e} + \tilde{K}e + \tilde{D}\dot{e} \tag{17}$$

with

$$\tilde{K} = K_{d1} - K,\ \tilde{D} = K_{d2} - D \tag{18}$$

In order to obtain stiffness K and damping D, we consider a Lyapunov function candidate

$$J_c = \frac{1}{\theta_k}\mathrm{vec}^T(\tilde{K})\mathrm{vec}(\tilde{K}) + \frac{1}{\theta_d}\mathrm{vec}^T(\tilde{D})\mathrm{vec}(\tilde{D}) \tag{19}$$

where θ_k and θ_d are positive parameters to adjust the stiffness and damping, respectively. By considering the time derivative of (19) (detailed derivations are found in the Appendix), K and D can be updated as

$$\dot{K} = \theta_k\dot{e}e^T,\ \dot{D} = \theta_d\dot{e}\dot{e}^T. \tag{20}$$

With the coordinate transformation in Sect. 2.2, the system dynamics are divided to a subspace along the predefined path and the other normal to it. Where it does not cause any confusion, we use subscripts "t" and "n" to denote tangential and normal components in the matrices and variables, respectively.

3.3 Trajectory learning

In the direction along the predefined task path, we want to achieve a constant level of assistance from the robot to the human, defined by a desired force f_{hdt}. By considering the model of human force in Eq. (11), we have

$$f_{hdt} = K_{ht}(X_{vt} - X_{hdt}) \tag{21}$$

where X_{vt} is a virtual trajectory that generates the desired force f_{hdt}. Since the human's parameters K_{ht} and X_{hdt} are unknown, X_{vt} cannot be computed directly. Therefore, we will develop a trajectory learning method to obtain it.

Combining Eqs. (11) and (21), we obtain

$$\Delta f_{hdt} = K_h\Delta X_{vt} \tag{22}$$

with

$$\Delta f_{hdt} = f_{ht} - f_{hdt},\ \Delta X_{vt} = X_t - X_{vt}. \tag{23}$$

Although X_{vt} is unknown to the robot, we can find that Δf_{hdt} is proportional to ΔX_{vt} according to Eq. (22). Inspired by this observation, a learning law is designed to obtain the robot's desired trajectory X_{dt} as below:

$$\Delta X_{dt}(t) = X_{dt}(t) - X_{dt}(t-T) = -\phi\Delta f_{hdt} \tag{24}$$

where ϕ is a positive learning rate. In other words, the desired trajectory is learned through minimizing the error between the desired force f_{hdt} and the actual one f_{ht}. The learning of X_d will converge when $f_{ht} = f_{hdt}$, i.e. when the desired interaction force in the tangential direction is achieved.

In summary, the proposed controller is designed with reference to a coordinate frame attached to the predefined task path. Adaptive impedance control is developed to guarantee the tracking performance in both normal and tangential directions. Trajectory learning is designed to provide a constant level of assistance by achieving the desired interaction force in the tangential direction. The proposed control scheme is presented in Fig. 3, with its performance analysis given in the "Appendix".

4 Experiments

4.1 Experimental setup

As shown in Fig. 4, the experimental platform contains an H-MAN robot (ARTICARES Pte Ltd), a force sensor and a control computer. H-MAN is utilized to physically interact

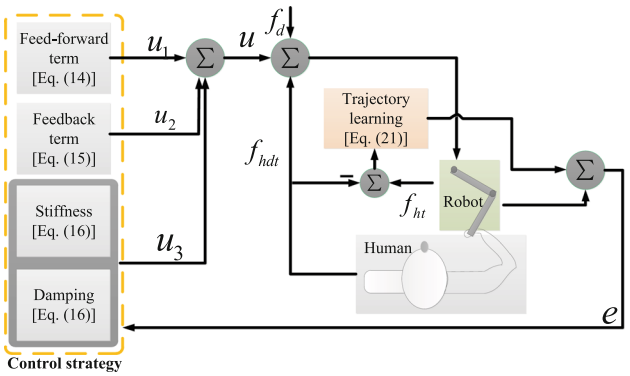

Fig. 3 Block diagram of the proposed control scheme for a rehabilitation robot: the yellow dotted block denotes the robot controller with feed-forward, feedback and impedance adaptation in order to guarantee the tracking performance; red block represents trajectory learning to guarantee a constant level of assistance with a desired force in the tangential direction

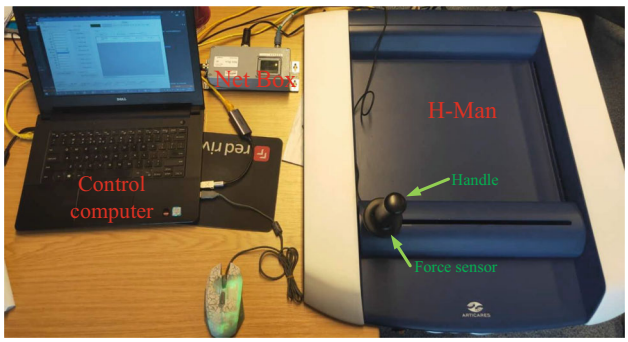

Fig. 4 Experiment platform

with the human user through the handle in a planar space. An ATI Mini-40 force/torque sensor is mounted on the handle of H-MAN. The force information is communicated with an ATI Net Box between the H-MAN and the control computer. All devices send the information to the control computer through a transmission control protocol.

Choosing the right exercise/training modes according to the human patients' recovery stage is important [37]. Upper-limb rehabilitation training modes can be divided into four main categories: passive, assistive, active and resistive modes [38]. In our experiments, three different modes were considered to represent typical tasks: zero interaction force mode, assistive mode with a negative desired force and resistive mode with a positive desired force. During the experiments, the human user was asked to follow a predefined path. At the same time, the robot's control objective was to guarantee the tracking of the predefined path and to provide a constant level of assistance to the human user along the path.

The robot's initial desired trajectory in Fig. 5 is defined as

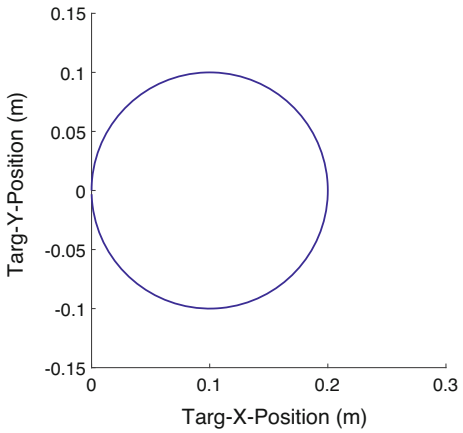

Fig. 5 Robot's initial desired trajectory

$$\begin{aligned} x_d &= A(1-\cos(\omega t)) \\ y_d &= A\sin(\omega t) \end{aligned} \tag{25}$$

where $A = 10$ cm, $\omega = 2\pi$ rad/s. This trajectory is updated in each cycle by Eq. (24) with $\phi = 0.004$.The robot's feedback gains are set as $K_p = 300$ N/m, $K_d = 100$ Ns/m. These impedance parameters are initiated as 0 and updated with factors $\theta_k = 1000$ and $\theta_d = 1000$, respectively, to guarantee the smooth interaction during the task. The desired interaction force in the tangential direction f_{hdt} is set in different modes as detailed in the following.

4.2 Zero interaction force mode

The experimental results of zero interaction force mode are shown in Fig. 6. In this mode, the desired interaction force was set to be 0N, in other words ideally the human user does not feel any force during the exercise along the given circular path after trajectory learning. To this end, trajectory learning was used to update the robot's desired trajectory in the tangential direction until it achieves the required interaction. Figure 6a shows the actual position of the robot during each cycle, converging to the predefined circular path. Figure 6b shows the normal direction tracking error reduces to small values, indicating the robot assisting the human user to stick to the predefined path. Figure 6c, d shows the velocity change in the tangential direction to match the human speed and thus the interaction force iteratively converges to about 0N. Figure 6e–f shows the impedance adaptation in both normal and tangential directions to keep the human movement close to the circular path. Note that the disturbance modelled by Eq. (12) is unknown in the experiments, but results of impedance adaptation have shown how the robot automatically updates its parameters to deal with the unknown disturbance and to guarantee the tracking performance.

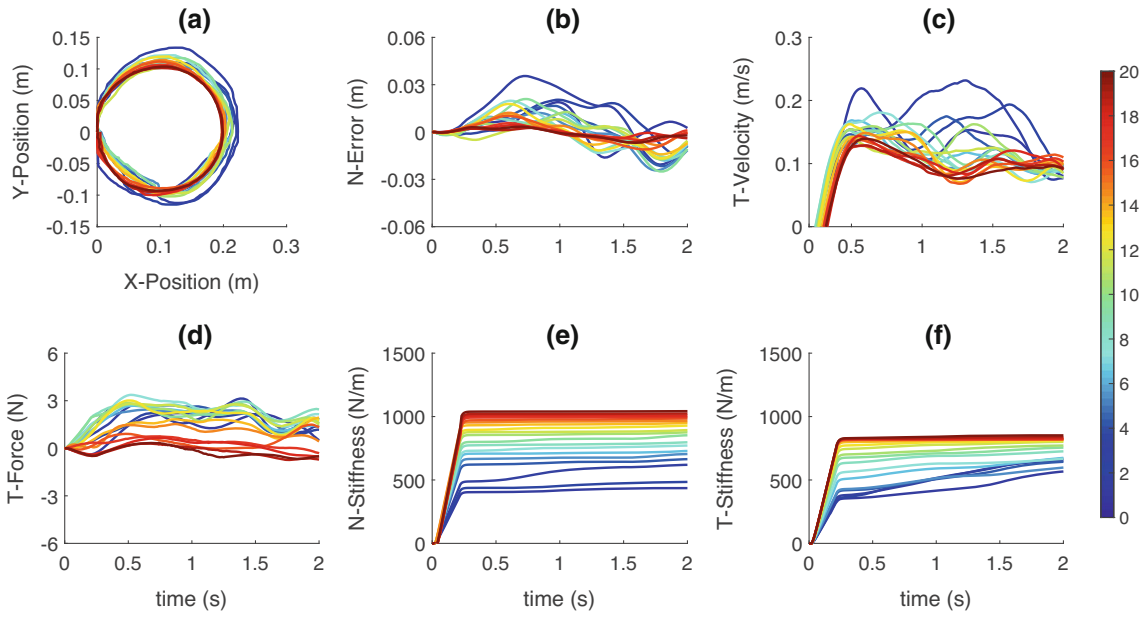

Fig. 6 Zero interaction force mode: **a** actual trajectory, **b** normal direction error, **c** tangential direction velocity, **d** tangential direction interaction force, **e** normal direction stiffness, **f** tangential direction stiffness. Different cycles are shown by the color bar, which changes from blue (cycle number $j = 1$) to red ($j = 20$)

4.3 Assistive mode

Assistive mode is usually used in initial recovery stage for motor dysfunction. Experimental results in this mode are presented in Fig. 7. Figure 7a shows how the human user followed the robot lead and completed the path following task. It can be seen that the robot did not go back to the initial position due to the slow movement of the human user. Nevertheless, the position error in the normal direction was significantly reduced as illustrated in Fig. 7b. In this mode, the robot's desired trajectory in the tangential direction was also automatically updated so the required velocity and interaction force of -2N were achieved, as shown in Fig. 7c–d. Figure 7e shows similar converging

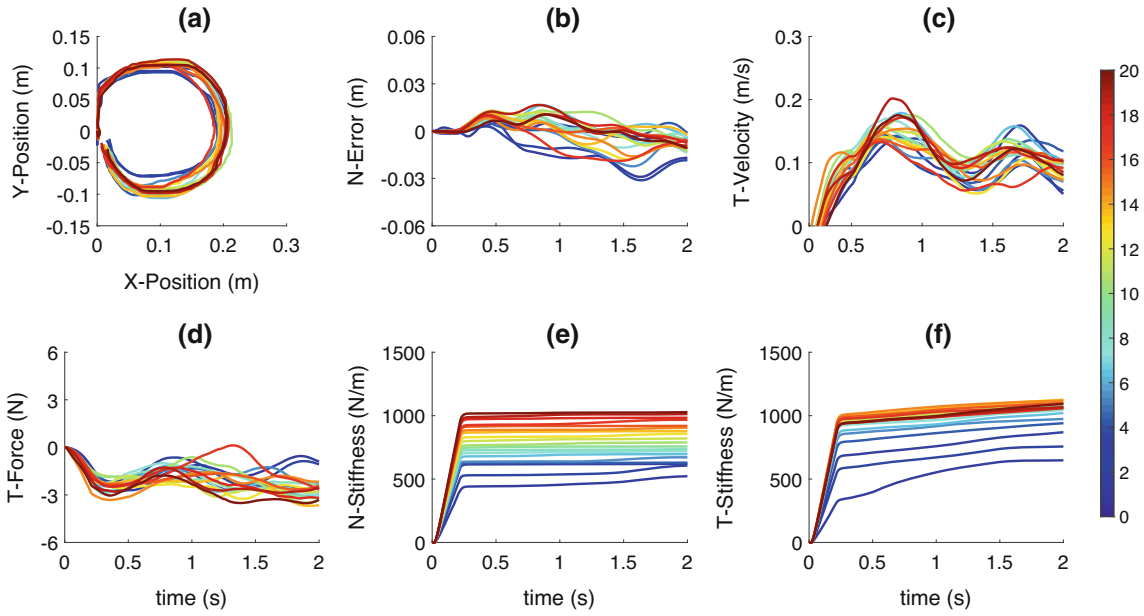

Fig. 7 Assistive interaction mode: **a** actual trajectory, **b** normal direction error, **c** tangential direction velocity, **d** tangential direction interaction force, **e** normal direction stiffness, **f** tangential direction stiffness. Different cycles are shown by the color bar, which changes from blue (cycle number $j = 1$) to red ($j = 20$)

stiffness values compared to that in the zero interaction force mode. However, Fig. 7f shows higher converging stiffness values compared to the counterpart in the zero interaction force mode. Due to the desired interaction force of −2N, it requires a higher stiffness to ensure trajectory tracking in the presence of human force. These results demonstrate how adaptive impedance control can automatically deal with different cases to ensure the tracking performance.

4.4 Resistive mode

In RAR, resistive mode plays a key role to promote motor learning in a later stage of recovery. This mode was emulated by setting a desired interaction force of 3N and the results are shown in Fig. 8. Similarly, Fig. 8a–f, respectively, illustrates the robot's actual position during exercise, normal direction position error reduced to a small value through impedance adaptation, velocity changed to match the human speed, tangential direction force converging to the desired value and stiffness parameters converging to a certain value. Compared to other two modes, the robot's velocity converges to a smaller value, indicating its attempt to resist the human user from reaching their desired speed.

4.5 Comparative analysis

To further explain the effectiveness of this proposed approach, fixed impedance control is used to perform experiments for above mentioned three modes of training. The robot's desired trajectory for fixed impedance control is the same as in Fig. 5 and its fixed impedance gains are set as $K_p = 300$ N/m, $K_d = 100$ Ns/m. The desired interaction force set in different modes is modulated by changing ω in Eq. (25). Before the experiments, ω is estimated when human user moves with the robot inactivated and the estimated value $\omega = 2\pi$ is used for zero interaction force mode. For assistive mode, ω is multiplied with a constant 1.07 and for resistive mode, ω is divided by 1.07. Figure 9 shows results with fixed impedance control in the above three modes of training. From Fig. 9a, d, fixed impedance control yields a larger normal position error and divergence of tangent force compared to results in Fig. 6b, d. Similarly, desired interaction force convergence is also not achieved in assistive and resistive modes in Fig. 9e, f with larger normal position errors in Fig. 9b, c, compared to results shown in Figs. 7 and 8. To conclude, as compared to fixed impedance control, iterative learning-based path control achieves convergence of interaction force and impedance adaptation ensures path following.

4.6 Multiple trials

Our approach is based on an assumption of consistent human movement. Although this assumption can be partly fulfilled by asking the human subject to repeat the same movement during each cycle, there exist inevitable uncertainties. In this subsection, more experiments with multiple trials were carried out to examine the robustness of the

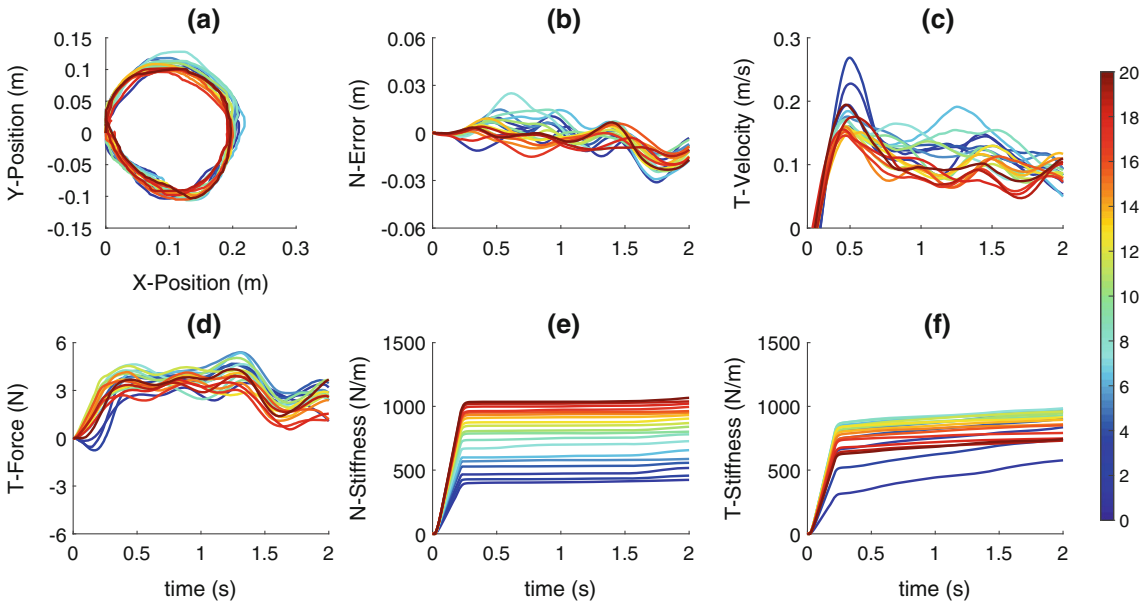

Fig. 8 Resistive interaction mode: **a** actual trajectory, **b** normal direction error, **c** tangential direction velocity, **d** tangential direction interaction force, **e** normal direction stiffness, **f** tangential direction stiffness. Different cycles are shown by the color bar, which changes from blue (cycle number $j = 1$) to red ($j = 20$)

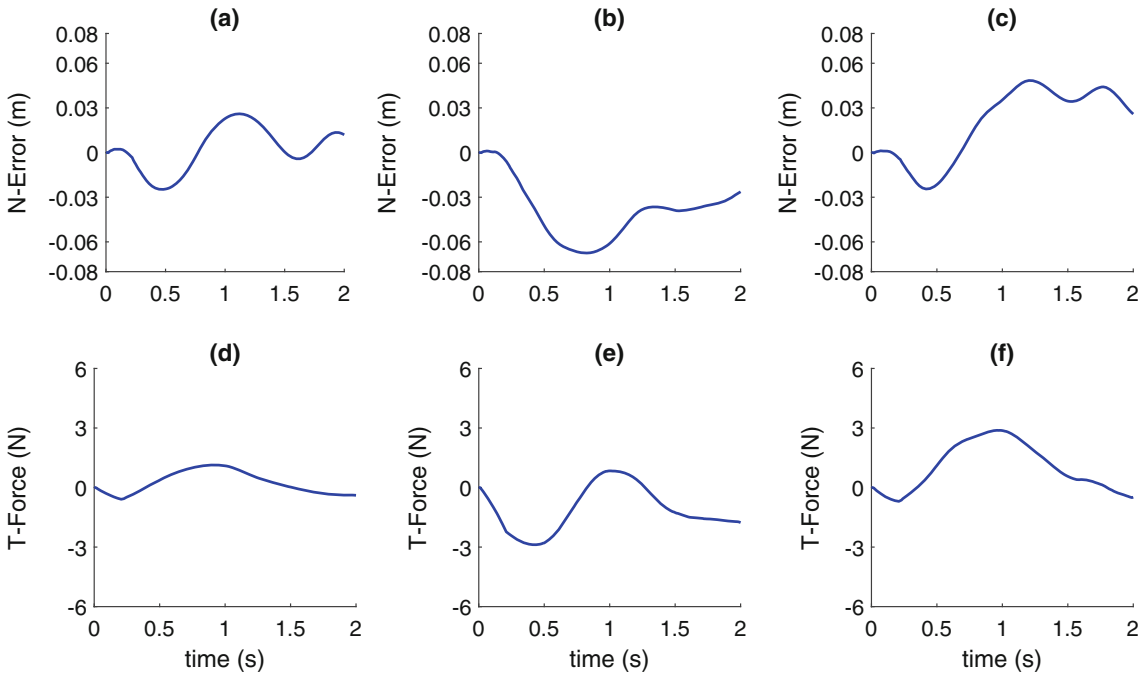

Fig. 9 Fixed impedance control: normal direction error and tangential direction interaction force in three modes: zero interaction force (**a**, **d**), assistive interaction (**b**, **e**) and resistive interaction (**c**, **f**)

proposed method against these uncertainties. Each mode was performed by the same human subject for five trials and each trial comprised of 20 cycles. In Figs. 10, 11, and 12, average values of 20 cycles for each trial are shown, including normal direction error, tangential direction force, normal direction stiffness and tangential direction stiffness. Average values are computed in each cycle, then the final average value for each trial is computed from 20 average values from all cycles in one trial. The values of stiffness in the normal and tangential directions show that the adaptive impedance control can update the stiffness according to different modes (subfigures (c),(d)) and ensure small normal direction errors (subfigure (a)) in all modes. In addition to this, the average values of interaction force show that different desired forces have been achieved (subfigure (b)) in each mode. In particular, Fig. 10b shows an interaction force between 0.5 and 1.1 N in the zero interaction force mode. The nonzero force is likely due to the friction that has not been compensated. Figure 11b shows an interaction force between $-(1.9-2.1)$N, which is close to the desired

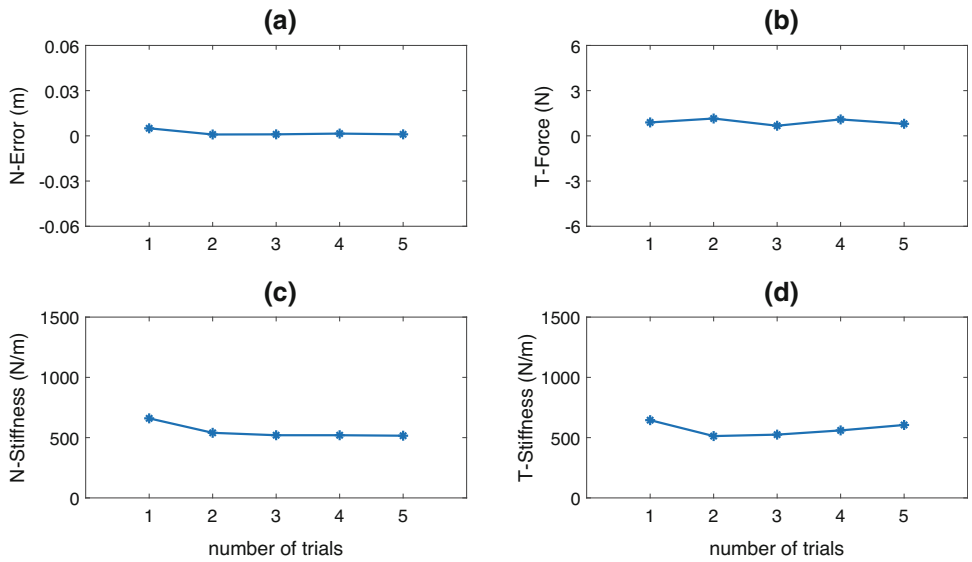

Fig. 10 Average values of 20 cycles for 5 trials in zero interaction force mode: **a** normal direction tracking error, **b** tangential direction interaction force, **c** normal direction stiffness, **d** tangential direction stiffness

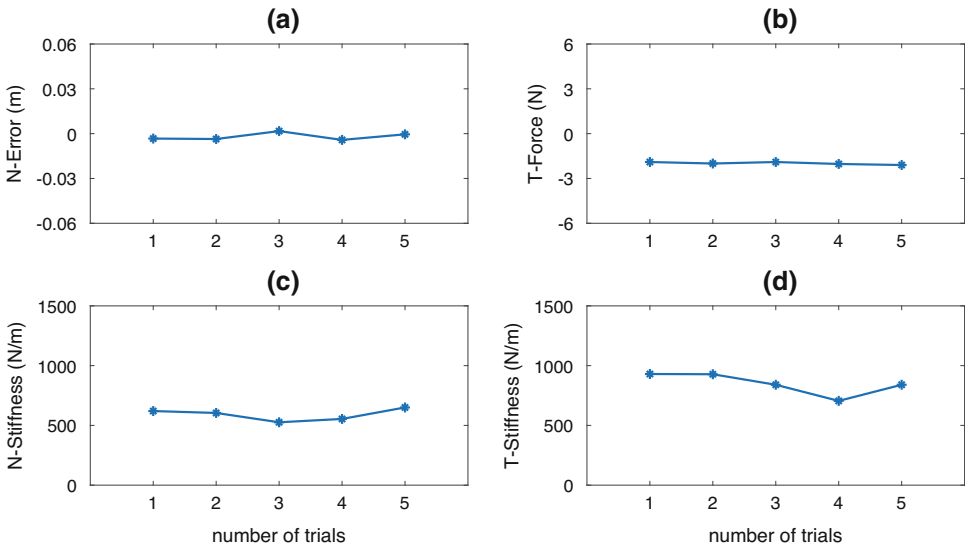

Fig. 11 Average values of 20 cycles for 5 trials in assistive interaction mode: **a** normal direction tracking error, **b** tangential direction interaction force, **c** normal direction stiffness, **d** tangential direction stiffness

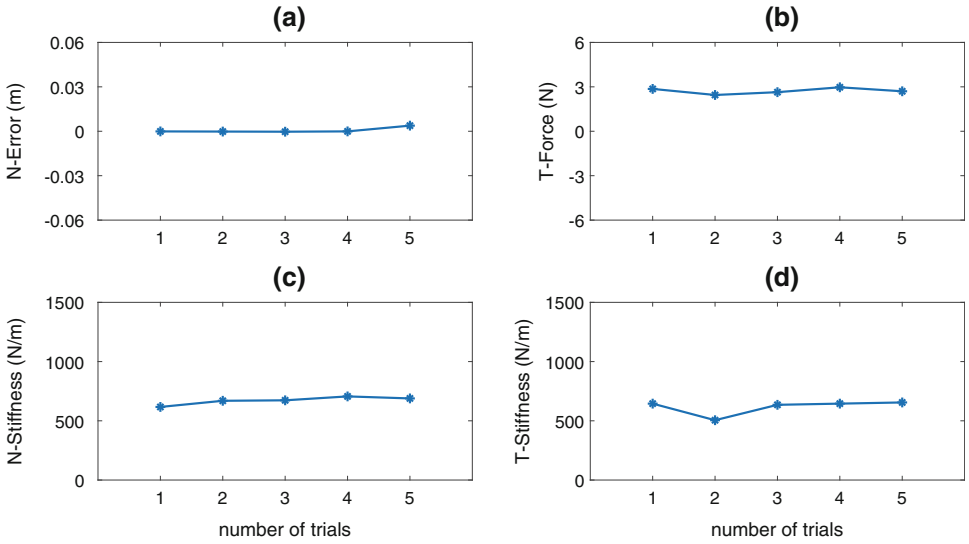

Fig. 12 Average values of 20 cycles for 5 trials in resistive interaction mode: **a** normal direction tracking error, **b** tangential direction interaction force, **c** normal direction stiffness, **d** tangential direction stiffness

value of − 2 N in the assistive mode. Figure 12b shows an interaction force between 2.6 and 3.1 N, which is also around the desired value of 3 N in the resistive mode.

Finally, we use one-way analysis of variance (ANOVA) to verify the differences of performance measures between three modes. The mean value and standard deviations of normal direction position errors and tangential direction forces in each mode were computed using 200 data points for each mode in five trials. Figure 13 shows that the tracking error in the normal direction has significant differences between zero interaction force mode and the other two modes. Larger tracking errors are due to nonzero interaction forces but their mean values are less than 0.3 cm, which is acceptable. Figure 13 also shows that the interaction force in the tangential direction has significant differences between different modes, indicating different desired levels of interaction. Above experimental results show that although human movement uncertainties exist, our approach ensures relatively consistent performance.

5 Conclusions

In this paper, a combined scheme of adaptive impedance control and trajectory learning is proposed and performed in a coordinate frame attached to a predefined path for RAR. In order to deal with the influence of unknown disturbances from the environment (including the human user) and the robotic system, we have proposed an updating law to adapt the robot's impedance. Considering different dynamics of the humans, a trajectory learning algorithm has been developed to provide a constant level of assistance for the repetitive training tasks in the tangential direction. The robot's trajectory can be updated based on

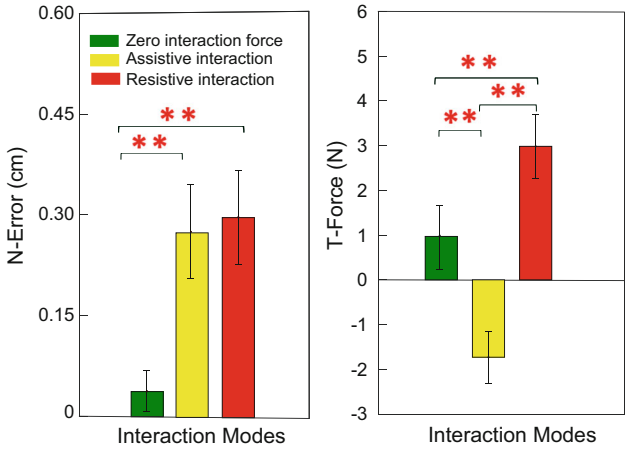

Fig. 13 The mean value and standard deviations of normal direction position errors and tangential direction forces in three modes. A single asterisk "*" indicates difference with $p<0.01$, and a double asterisk "**" indicates significant difference with $p<0.001$

the interaction force iteratively for the next circle. Stability and convergence of the proposed adaptive impedance control and trajectory learning have been proved in theory. The validation of the proposed approach has been performed by comparative experiments in different interaction modes. Further analysis has been also performed with multiple trials to demonstrate its robustness. Future works include test and improvement of the proposed approach in real clinic trials with human patients. Moreover, multiple robots assisting in completing a common task, i.e. the distributed collaborative optimization problem, will be also studied for RAR [39, 40].

Appendix

The whole control scheme includes two main parts: adaptive impedance controller and trajectory learning. Impedance parameters adaptation is considered in both the normal and tangential directions, with an aim to guarantee the tracking performance, i.e. when $t \to \infty$, $e_t \to 0, e_n \to 0$. Trajectory learning is considered in the tangential direction to obtain the desired trajectory for achieving a desired interaction force, i.e. when $t \to \infty$, $f_{ht} = f_{hdt}$. Let us first consider the adaptive impedance control, by defining

$$J = J_c + J_e \tag{26}$$

where J_c has been defined in (19) and J_e is given by

$$J_e = \frac{1}{2}\dot{e}^T M_d \dot{e} + \frac{1}{2} e^T K_p e. \tag{27}$$

Taking the time derivative of (19), we have

$$\begin{aligned} \dot{J}_c &= \mathrm{tr}\left(\frac{1}{\theta_k}\tilde{K}^T\dot{\tilde{K}} + \frac{1}{\theta_d}\tilde{D}^T\dot{\tilde{D}}\right) \\ &= -\mathrm{tr}\left(\frac{1}{\theta_k}\tilde{K}^T\theta_k e e^T + \frac{1}{\theta_d}\tilde{D}^T\theta_d e\dot{e}^T\right) \\ &= -\mathrm{tr}\left(\tilde{K}^T\dot{e}e^T + \tilde{D}^T\dot{e}\dot{e}^T\right) \\ &= -\dot{e}^T\left(\tilde{K}e + \tilde{D}\dot{e}\right). \end{aligned} \tag{28}$$

Taking the time derivative of (27) and considering the closed-loop dynamics (17), we have

$$\begin{aligned} \dot{J}_e &= \dot{e}^T M_d \ddot{e} + \frac{1}{2}\dot{e}^T\dot{M}_d\dot{e} + e^T K_p\dot{e} \\ &= \dot{e}^T M_d\ddot{e} + \dot{e}^T B_d\dot{e} + e^T K_p\dot{e} \\ &= \dot{e}^T(-K_d\dot{e} + \tilde{K}e + \tilde{D}\dot{e}) \end{aligned} \tag{29}$$

By combining Eqs. (28) and (29), we have

$$\dot{J}_c + \dot{J}_e = -\dot{e}^T K_d\dot{e} \le 0 \tag{30}$$

Therefore, when $t \to \infty$, $\dot{e} \to 0$. According to Eq. (17), we have $e \to 0$. For the trajectory learning in the tangential direction, another Lyapunov function candidate is defined as

$$J_{rt} = \frac{1}{2\phi}\int_{t-T}^{t}\{(X_{dt} - X_{vt})^T(X_{dt} - X_{vt})\}d\tau \tag{31}$$

Then, the difference between J_{rt} in two cycles is

$$\Delta J_{rt} = J_{rt}(t) - J_{rt}(t-T). \tag{32}$$

After further expanding Eq. (32), we have

$$
\begin{aligned}
\Delta J_{rt} = \frac{1}{2\phi}\Bigg\{ & \int_{t-T}^{t} (X_{dt}(\tau) - X_{vt}(\tau))^T (X_{dt}(\tau)) d\tau \\
& - \int_{t-T}^{t} (X_{vt}(\tau) - (X_{dt}(\tau) - X_{vt}(\tau))^T \\
& \times (X_{dt}(\tau - T)) - X_{vt}(\tau - T) + X_{dt}(\tau)) d\tau \\
& - \int_{t-T}^{t} (X_{vt}(\tau - T) - X_{dt}(\tau - T)) d\tau \\
& - \int_{t-T}^{t} (X_{vt}(\tau))^T (X_{dt}(\tau - T))) d\tau \\
& - \int_{t-T}^{t} X_{vt}(\tau - T))^T (X_{dt}(\tau - T) d\tau \\
& - \int_{t-T}^{t} X_{vt}(\tau - T)) d\tau \Bigg\} \\
= \frac{1}{2\phi}\Bigg\{ & \int_{t-T}^{T} (X_{dt}(\tau) d\tau - \int_{t-T}^{t} X_{vt}(\tau))^T \Delta X_{dt}(\tau) d\tau \\
& + \int_{t-T}^{t} (X_{dt}(\tau - T) - X_{vt}(\tau - T))^T \\
& \times \Delta X_{dt}(\tau - T) d\tau \} \\
= \frac{1}{\phi}\Bigg\{ & \int_{t-T}^{t} (X_{dt}(\tau) - X_{vt}(\tau) - \frac{1}{2}\Delta X_{dt}(\tau))^T \\
& \times \Delta X_{dt}(\tau) d\tau \} \leqslant \frac{1}{\phi} \{ \int_{t-T}^{t} X_{dt}(\tau) d\tau \\
& - \int_{t-T}^{t} (X_{vt}(\tau))^T \Delta X_{dt}(\tau) d\tau \} \\
= \frac{1}{\phi} \{ & \int_{t-T}^{t} (X_{dt}(\tau) - X_t(\tau) + X_t(\tau) - X_{vt}(\tau))^T \\
\times \Delta X_{dt}(\tau) d\tau \} \leqslant \frac{1}{\phi} \{ & \int_{t-T}^{t} (-e_t(\tau) + X_t(\tau) - X_{vt}(\tau))^T \\
& \times \Delta X_{dt}(\tau) d\tau \}
\end{aligned}
\tag{33}
$$

where we have used $X_{vt}(t) = X_{vt}(t - T)$. By considering Eq. (22) and $e_t(t) \to 0$, we further have

$$
\begin{aligned}
\Delta J_{rt}; \leqslant - \int_{t-T}^{t} & \{K_{ht}^{-1} (f_{ht}(\tau) - f_{hdt}(\tau))^T \\
& \times (f_{ht}(\tau) - f_{hdt}(\tau))\} d\tau \leqslant 0.
\end{aligned}
\tag{34}
$$

Therefore, when $t \to \infty$, $f_{ht} = f_{hdt}$, indicating the desired force is achieved in the tangential direction.

Ackowledgements This research was supported in part by the UK EPSRC Grant (EP/T006951/1) and the Open Research Project of the State Key Laboratory of Industrial Control Technology, Zhejiang University, China (ICT20050).

Declarations

Conflict of interest The authors declare that they have no conflict of interest.

Open Access This article is licensed under a Creative Commons Attribution 4.0 International License, which permits use, sharing, adaptation, distribution and reproduction in any medium or format, as long as you give appropriate credit to the original author(s) and the source, provide a link to the Creative Commons licence, and indicate if changes were made. The images or other third party material in this article are included in the article's Creative Commons licence, unless indicated otherwise in a credit line to the material. If material is not included in the article's Creative Commons licence and your intended use is not permitted by statutory regulation or exceeds the permitted use, you will need to obtain permission directly from the copyright holder. To view a copy of this licence, visit http://creativecommons.org/licenses/by/4.0/.

References

1. W. S. Organization, "Vision and strategy," https://www.world-stroke.org/about-wso/vision-and-strategy
2. Helgason CM, Wolf PA (1997) American heart association prevention conference iv: prevention and rehabilitation of stroke: executive summary. Circulation 96(2):701–707
3. Lewis GN, Rosie JA (2012) Virtual reality games for movement rehabilitation in neurological conditions: how do we meet the needs and expectations of the users? Disabil Rehabilit 34(22):1880–1886
4. Fang X-K, Han B, Wang J-H, Liu D-Y (2016) Adaptive velocity field control of upper-limb rehabilitation robot. In: *2016 Chinese Control and Decision Conference (CCDC)*. IEEE, pp 5438–5443
5. Frisoli A, Salsedo F, Bergamasco M, Rossi B, Carboncini MC (2009) A force-feedback exoskeleton for upper-limb rehabilitation in virtual reality. Appl Bionics Biomech 6(2):115–126
6. Zhang J, Cheah CC (2015) Passivity and stability of human-robot interaction control for upper-limb rehabilitation robots. IEEE Trans Robot 31(2):233–245
7. Zhang J, Cheah CC, Collins SH (2013) Stable human-robot interaction control for upper-limb rehabilitation robotics. In: *2013 IEEE International Conference on Robotics and Automation*. IEEE, pp 2201–2206
8. Luo J, Lin Z, Li Y, Yang C (2020) A teleoperation framework for mobile robots based on shared control. IEEE Robot Auto Lett 5(2):377–384
9. Luo J, Yang C, Wang N, Wang M (2019) Enhanced teleoperation performance using hybrid control and virtual fixture. Int J Syst Sci 50(3):451–462
10. Hogan N (1984) Impedance control: an approach to manipulation. In: *1984 American Control Conference*. IEEE, pp 304–313
11. Shi G, Xu G, Wang H, Duan N, Zhang S (2019) Fuzzy-adaptive impedance control of upper limb rehabilitation robot based on semg. In: *2019 16th International Conference on Ubiquitous Robots (UR)*. IEEE, pp 745–749
12. Huang Y, Su SW, Song R (2020) Voluntary intention-driven rehabilitation robots for the upper limb. In: *Intelligent Biomechatronics in Neurorehabilitation*. Elsevier, pp 111–130
13. Khairuddin IM, Na'im Sidek S, Majeed APA, Puzi AA, Yusof HM (2020) A hybrid automata framework for an adaptive impedance control of a robot-assisted training system. In: *RITA 2018*, Springer, pp 257–265
14. Aktan ME, Akdoğan E (2018) Design and control of a diagnosis and treatment aimed robotic platform for wrist and forearm rehabilitation: diagnobot. Adv Mech Eng 10(1):1687814017749705
15. Yu H, Huang S, Chen G, Pan Y, Guo Z (2015) Human-robot interaction control of rehabilitation robots with series elastic actuators. IEEE Trans Robot 31(5):1089–1100

16. Li X, Pan Y, Chen G, Yu H (2016) Adaptive human-robot interaction control for robots driven by series elastic actuators. IEEE Trans Robot 33(1):169–182
17. Yang C, Huang K, Cheng H, Li Y, Su C-Y (2017) Haptic identification by elm-controlled uncertain manipulator. IEEE Trans Syst Man Cybern Syst 47(8):2398–2409
18. Luo J, Yang C, Burdet E, Li Y (2020) Adaptive impedance control with trajectory adaptation for minimizing interaction force. *2020 IEEE International Symposium on Robot and Human Interactive Communication*, pp 1–6
19. Kronander K, Billard A (2016) Stability considerations for variable impedance control. IEEE Trans Robot 32(5):1298–1305
20. Zeng C, Yang C, Cheng H, Li Y, Dai S-L (2020) Simultaneously encoding movement and semg-based stiffness for robotic skill learning. IEEE Trans Ind Inf 17(2):1244–1252
21. Li Z, Huang Z, He W, Su C-Y (2016) Adaptive impedance control for an upper limb robotic exoskeleton using biological signals. IEEE Trans Ind Electr 64(2):1664–1674
22. Wu Q, Wang X, Chen B, Wu H (2017) Development of a minimal-intervention-based admittance control strategy for upper extremity rehabilitation exoskeleton. IEEE Trans Syst Man Cybern Syst 48(6):1005–1016
23. Chi R, Hou Z, Xu J (2008) Adaptive ilc for a class of discrete-time systems with iteration-varying trajectory and random initial condition. Automatica 44(8):2207–2213
24. Losey DP, O'Malley MK (2019) Learning the correct robot trajectory in real-time from physical human interactions. ACM Trans Hum-Robot Interact (THRI) 9(1):1–19
25. Chen G, Yuan B, Jia Q, Fu Y, Tan J (2019) Trajectory optimization for inhibiting the joint parameter jump of a space manipulator with a load-carrying task. Mech Mach Theory 140:59–82
26. Agarwal P, Deshpande AD (2017) Subject-specific assist-as-needed controllers for a hand exoskeleton for rehabilitation. IEEE Robot Auto Lett 3(1):508–515
27. Hussain S, Jamwal PK, Ghayesh MH, Xie SQ (2016) Assist-as-needed control of an intrinsically compliant robotic gait training orthosis. IEEE Trans Ind Electr 64(2):1675–1685
28. Shahbazi M, Atashzar SF, Tavakoli M, Patel RV (2016) Robotics-assisted mirror rehabilitation therapy: a therapist-in-the-loop assist-as-needed architecture. IEEE/ASME Trans Mech 21(4):1954–1965
29. Yang C, Chen C, He W, Cui R, Li Z (2018) Robot learning system based on adaptive neural control and dynamic movement primitives. IEEE Trans Neural Netw Learn Syst 30(3):777–787
30. Zhou S-H, Oetomo D, Tan Y, Burdet E, Mareels I (2012) Modeling individual human motor behavior through model reference iterative learning control. IEEE Trans Biomed Eng 59(7):1892–1901
31. Ajjanaromvat N, Parnichkun M (2018) Trajectory tracking using online learning lqr with adaptive learning control of a leg-exoskeleton for disorder gait rehabilitation. Mechatronics 51:85–96
32. Ghanbari V, Duenas VH, Antsaklis PJ, Dixon WE (2018) Passivity-based iterative learning control for cycling induced by functional electrical stimulation with electric motor assistance. IEEE Trans Control Syst Technol 27(5):2287–2294
33. Huo F, Poo A-N (2013) Precision contouring control of machine tools. Int J Adv Manuf Technol 64(1–4):319–333
34. Liu Y, Cong S (2009) Optimal contouring control based on task coordinate frame and its simulation. J Syst Simul 21(11):229–234
35. Wang Z, Hu C, Zhu Y, He S, Zhang M, Mu H (2017) Newton-ilc contouring error estimation and coordinated motion control for precision multiaxis systems with comparative experiments. IEEE Trans Ind Electr 65(2):1470–1480
36. Lou Y, Chen N, Li Z (2006) Task space based contouring control of parallel machining systems. In: *2006 IEEE/RSJ International Conference on Intelligent Robots and Systems*. IEEE, pp 2047–2052
37. Huang X, Naghdy F, Naghdy G, Du H, Todd C (2017) Robot-assisted post-stroke motion rehabilitation in upper extremities: a survey. Int J Disabil Hum Dev 16(3):233–247
38. Li C, Rusák Z, Horváth I, Ji L, Hou Y (2014) Current status of robotic stroke rehabilitation and opportunities for a cyber-physically assisted upper limb stroke rehabilitation. Proc TMCE 1:899–914
39. Lü Q, Liao X, Li H, Huang T (2020) Achieving acceleration for distributed economic dispatch in smart grids over directed networks. IEEE Trans Netw Sci Eng 7(3):1988–1999
40. Lü Q, Liao X, Xiang T, Li H, Huang T (2020) Privacy masking stochastic subgradient-push algorithm for distributed online optimization. IEEE Trans Cybern. https://doi.org/10.1109/TCYB.2020.2973221

Publisher's Note Springer Nature remains neutral with regard to jurisdictional claims in published maps and institutional affiliations.